Binding of methimazole and NADP(H) to human FMO3: In vitro and in silico studies

Abstract

Human flavin-containing monooxygenase isoform 3 (hFMO3) is an important hepatic drug-metabolizing enzyme, catalyzing the monooxygenation of nucleophilic heteroatom-containing xenobiotics. Based on the structure of bacterial FMO, it is proposed that a conserved asparagine is involved in both NADP(H) and substrate binding. In order to explore the role of this amino acid in hFMO3, two mutants were constructed. In the case of N61Q, increasing the steric hindrance above the flavin N5-C4a causes poor NADP(H) binding, destabilizing the catalytic FAD intermediate, whereas the introduction of a negatively charged residue, N61D, interferes mainly with catalytic intermediate formation and its stability. To better understand the substrate-enzyme interaction, *in vitro* as well as *in silico* experiments were carried out with methimazole as substrate. Methimazole is a high-affinity substrate of hFMO3 and can competitively suppress the metabolism of other compounds. Our results demonstrate that methimazole Pi-stacks above the isoalloxazine ring of FAD in hFMO3, in a similar way to indole binding to the bacterial FMO. However, for hFMO3 indole is found to act as a non-substrate competitive inhibitor. Finally, understanding the binding mode of methimazole and indole could be advantageous for development of hFMO3 inhibitors, currently investigated as a possible treatment strategy for atherosclerosis.

Keywords

Human flavin-containing monooxygenase isoform 3, active site mutant, methimazole, calorimetry, molecular docking.

Abbreviations

hFMO3, Human flavin-containing monooxygenase isoform 3; Methimazole, MMI; ITC, Isothermal Titration Calorimetry; DSC, Differential Scanning Calorimetry

1. Introduction

During the last few decades a large number of flavin-containing monooxygenases (FMOs) have been studied revealing their specificity to catalyze a wide range of oxidative reactions, which makes this class of enzymes of great interest for synthetic as well as biotechnological applications both in the chemical and medical fields [1-4]. One member of this class, human flavin-containing monooxygenase isoform 3 (hFMO3), is involved in the metabolism of a wide variety of nitrogen- and sulfur-containing chemicals [2, 5].

In general terms, the FMO catalytic cycle includes flavin reduction by NADPH, O_2 diffusion/activation, C4a-(hydro)peroxyflavin intermediate formation, substrate oxidation and finally, flavin regeneration [6]. The oxidized flavin prosthetic group is reduced by NADPH through a hydride transfer giving rise to the reduced flavin and $NADP^+$ [6]. For FMO, conformational changes and sidechain movements are thought to occur to accommodate the binding of NADPH and the subsequent flavin reduction [7].

The reduced flavin will further react with O_2 to form the C4a-hydrperoxyflavin intermediate which must be protected from decay in order to further react with the substrate otherwise the uncoupling reaction will result in hydrogen peroxide formation [8]. Flavoproteins adopt different mechanisms to provide an ideal physicochemical environment for the formation and most importantly the stabilization of C4a-(hydro)peroxyflavin intermediate. In FMO, after flavin reduction, $NADP^+$ remains bound to the enzyme. The nicotinamide ring of $NADP^+$ is stacked with the isoalloxazine ring and its amide nitrogen within hydrogen-bond distance from the flavin N5-H [7, 9]. Once formed, the C4a-(hydro)peroxyflavin oxygenates the substrate to yield the product.

Collectively in FMO, the flavoprotein-mediated catalytic reaction is primarily controlled and modulated by NADPH binding for the flavin reduction and $NADP^+$ binding for the C4a-hydrperoxyflavin intermediate stability.

To date, there are only two FMO proteins with known crystal structure, bacterial FMO from *Methylophaga* sp. Strain SK1 (bFMO) [7] and yeast FMO from *schizosaccharomyces pombe* (yFMO) [9], showing a catalytic microenvironment

in the presence of 0, 1, 2, 4 mM indole, respectively. The N-oxidize products were analyzed colorimetrically by monitoring the absorbance at 412 nm, 37 °C.

bFMO can oxygenate the indole to produce indoxyl followed by a non-enzymatic reaction to yield the indigo [20]. Here, HPLC (Agilent-1200, Agilent Technologies, U.S.A.) analysis was used to confirm if indole is a hFMO3 substrate. The reaction mixture contained 1 μM WT-hFMO3, 0.5 mM indole and 1 mM NADPH, 50 mM phosphate buffer (pH 7.4), in a total volume of 200 μl. The reactions were performed at 37 °C for 30 minutes before termination by 100 μl ice-cold acetonitrile. The resulting reaction mixture was analyzed by HPLC equipped with 4.6 × 150 mm 5 μm Eclipse XDB-C18 column, at room temperature. The mobile phases consisted of 45% acetonitrile and 55 % 0.1% formic acid in water, and an isocratic elution was used. Same experiments performed in the absence of WT-hFMO3 were used as the control.

The presence of substrate accelerates NADPH consumption in WT-hFMO3. Therefore, NADPH consumption in the absence and presence of indole was monitored at 340 nm spectrophotometrically. In detail, the reaction mixture contained 50 mM phosphate buffer (pH 7.4), 0.8 μM WT-hFMO3, 0.2 mM NADPH in the presence of 0, 2, 4 mM indole, respectively.

The type of inhibitory effect of indole on wild-type hFMO3-mediated methimazole S-oxidation was determined by Lineweaver-Burk plot. The reaction mixture consisted of different concentrations of MMI (0.02-0.32 mM), 60 μM DTNB, 30 μM DTT, 0.82 μM hFMO3, 0.5 mM NADPH, 50 mM phosphate buffer (pH 7.4), in the presence of different concentrations of indole (0, 1, 2, 3 mM). The absorbance changes were recorded at 412 nm.

2.3. *In silico* mutagenesis and molecular docking

Structural views of MMI and NADP(H) binding modes to the protein were explored by molecular docking experiments. As the 3D structure of hFMO3 is not available, a structural model built by homology modelling was used as the template for *in silico* mutation [21]. The templates used for the latter 3D model were bFMO (with 23.0% sequence identity and 40.4% sequence homology to hFMO3) [7] and yFMO (with 21.5%

sequence identity and 37.5% sequence homology to hFMO3) [9]. The “swap” function in YASARA [22] was used to generate the N61D and N61Q mutants. The mutated residue was then optimized by screening of the rotamer libraries to fully relax the steric clashes. The refined mutant models were docked with NADP(H) and MMI to investigate the changes of catalytic pocket shape and NADP(H) binding modes after mutation, and the results were analyzed by Discovery Studio Visualizer (DS Visualizer). The NADPH, $NADP^+$ and MMI used for molecular docking were prepared from the crystal structures of *pc*DHFR (PDB ID: 4IXE) [23], bFMO (PDB ID: 2VQ7) [7] and yFMO (PDB ID: 2GVC) [9], respectively and, the docking experiments were performed by YASARA Structure package [22]. For $NADP^+$ and MMI, prior to the docking experiments, dioxygen binding at the C4a position of FAD was modelled [7] and optimized by multiple Clean Geometry function in DS Visualizer. The docking procedure includes a global docking experiment followed by a local docking yielding the final docking result as described previously [21], and the best docking mode with the highest binding energy was finally selected and subjected to energy minimization using YASARA Structure package.

In general, using YASARA, docking runs of the ligand to receptor yield results sorted by binding energy where more positive energies indicate stronger binding and negative energies equate to no binding. After global docking the best binding mode (pose) was selected based on the best binding energy. The complexes were then subjected to 999 runs of Local Docking yielding the final docked binding modes.

2.4. NADPH binding assay

Steady-state activity of NADPH oxidase for WT-hFMO3, N61D and N61Q mutants were determined spectrophotometrically by monitoring the decrease of NADPH with time at 340 nm. The reaction mixture contained 50 mM phosphate buffer pH 7.4, 0.2 μM enzyme with various concentrations of NADPH. Reactions were carried out at 37 °C for 20 min.

The pre-steady-state activity of NADPH oxidase for WT-hFMO3, N61D and N61Q mutants were determined by a stopped-flow apparatus (SF-61, HI-TECH scientific, UK) equipped with a diode array detector. The kinetic parameters of flavin reduction were

determined in an anaerobic glove box (Belle Technology, UK) by mixing 20 μM protein with various concentrations of NADPH using the stopped-flow instrument as previously described [19, 24]. Spectra (300 - 700 nm) were collected over time and the absorbance changes at 450 nm were analysed by Kinetic Studio Version 3.0 software package resulting in the rates of flavin reduction. Kinetic parameters were determined from the reaction rates with corresponding NADPH concentrations fitted to equation 1 using non-linear regression analysis (SigmaPlot 12.0).

$$k_{obs} = \frac{k_{\mathrm{red}}[\mathrm{NADPH}]}{K_{\mathrm{d}}+[\mathrm{NADPH}]} \quad \text{(Eq. 1)}$$

2.5. $NADP^+$ binding assay

Association constant (Ka) of $NADP^+$ to the mutants was determined by ITC experiments performed with the ITC_{200} calorimeter (Malvern, USA). The experiments were performed by titration of $NADP^+$ (20 mM for N61D and 2 mM for N61Q) into a 20 μM protein solution as described previously [19]. The experimental data were corrected for the heat of dilution of $NADP^+$ solution by performing separate titrations against only buffer. The results were analyzed by nonlinear regression using “One Set of Sites curve” fitting model (MicroCal iTC200 Origin) resulting in the calculated value of Ka. Finally, the dissociation constant (Kd) was calculated as it is equal to the inverse of the Ka values.

$NADP^+$ binding affinity in FMO is associated with the intermediate stability. The C4a-hydroperoxyflavin intermediate is monitored by the stopped-flow apparatus. The enzyme was first fully reduced by equimolar amounts of NADPH under anaerobiosis, then mixed with air-saturated buffer and monitored over time by stopped-flow. The data were subsequently analyzed by Kinetic Studio Version 3.0 software package.

3. Results

3.1. Purification of mutants and Tm measurements

WT-hFMO3 and its two mutants were heterologously expressed in *E. coli* and purified using protocols previously reported [17, 18]. The mutants were successfully

purified (Fig. S1) with yields of 9.6 and 8.5 mg per litre of culture for N61Q and N61D, respectively. On average the purified mutants had a purity index, A280/A450, of around 11 similar to the data of the WT-hFMO3.

The purified proteins were initially characterized spectrophotometrically. Fig. 1 shows the UV-vis spectra of WT-hFMO3, N61Q and N61D with the maxima around 375 and 450 nm. The mutant spectra are very similar to those of the WT-hFMO3 indicating that the mutations have not affected the FAD incorporation in the protein.

After the initial UV-vis characterization of the mutants, the thermostability of the purified proteins was determined by DSC as mentioned in Materials and Methods section. For all three proteins, a single symmetrical peak was not observed suggesting that the thermal unfolding of hFMO3 and its mutants is not a simple two-state process (Table S1- according to Lepock et al. [25] and Vermeer & Norde, [26]) and, in line with already published data for the WT-hFMO3 [19]. Two melting temperatures were obtained for each mutant after deconvolution of the thermographs (Fig. S2) and are reported in Table 1. As can be seen in Table 1, the calculated T_{m1} values are the same for WT and mutant hFMO3, around 45°C. However, both mutants show a slight increase in T_{m2} values compared to the WT-hFMO3. At present, we do not have a conclusive answer as to the origin of these two Tm values. In general, this observation indicates the existence of two underlying melting processes which may be related to two different domains ($NADP^+$ binding domain and FAD binding domain) of hFMO3 molecule [21], or the presence of two protein populations (native plus aggregated forms). More studies need to be carried out to clarify this point.

Table 1 The melting temperatures of WT-hFMO3, N61Q and N61D.

Enzyme	T_{m1}, °C	T_{m2}, °C
WT [19]	45.1 ± 0.1	49.0 ± 0.2
N61D	45.4 ± 0.1	50.6 ± 0.3
N61Q	45.7 ± 0.2	51.7 ± 0.2

3.2. Characterization of methimazole binding by molecular docking, fluorescent and competitive displacement assays

In the first set of experiments, in order to determine the catalytic activity of the purified mutant proteins, a well-known hFMO3 substrate, methimazole [27], was selected. The kinetic parameters for N61D- and N61Q-mediated methimazole S-oxygenation were determined following procedures outlined in the Materials and Methods section. Table 2 summarizes the data obtained in comparison to previously published data on WT-hFMO3. As can be seen in Table 2, although some activity was measurable (Fig. S3), both mutants display a significant decrease in catalytic efficiency. In addition, a tertiary amine, trimethylamine, another well-known substrate of hFMO3 [27, 28] was also tested, and in this case no N-oxygenated product was detected for any of the mutants (data not shown).

Table 2 Kinetic parameters of WT hFMO3 and its mutants toward methimazole S-oxidation

Enzyme	K_m (μM)	k_{cat} (min^{-1})	k_{cat}/K_m
WT [19]	14.9 ± 2.0	8.4 ± 0.9	0.56
N61D	5815.6 ± 2244.7	2.1± 0.2	0.00037
N61Q	2424.2 ± 523.5	4.2 ± 0.2	0.0017

In vitro steady-state kinetic experiments demonstrated significantly lower activity of these two mutants toward methimazole. In order to investigate if this arises from different substrate binding modes, WT-hFMO3 and the two mutants were docked with methimazole. Fig. 2a-c illustrate the best docking modes of each of the 3 proteins with methimazole. In all cases, methimazole interacts with the flavin isoalloxazine ring by Pi-stacking interaction(s). This type of Pi-Pi interaction has also been seen in the co-crystal structures of bFMO with indole (PDB ID: 2XVJ) (Fig. 3a) and yFMO with methimazole (PDB ID: 2GVC) (Fig. 3b). For completeness, the same Pi-Pi interactions have also been shown in Fig. 3C with the hFMO3 model docked with methimazole.

The methimazole binding mode was further explored by *in vitro* experiments using

the purified enzymes. Binding of methimazole above the isoalloxazine ring in hFMO3 can induce FAD fluorescence changes (quenching) which are reported in Fig. 2 d-f. As expected, the fluorescence of the protein-bound FAD is already largely quenched by the surrounding protein matrix, and only slightly quenched after methimazole addition. Fig. 2a-b shows that, in WT-hFMO3 and N61Q mutant, methimazole binds above FAD and parallel to the isoalloxazine ring, maximizing the overlap of the Pi system. In these two proteins, titration with increasing amounts of methimazole leads to even more quenching and therefore a decrease in the fluorescence signal (Fig. 2d and 2e). While for N61D mutant, Fig. 2c shows that methimazole adopts a T-shaped Pi-stacking interaction, which results in no further quenching or decrease in the fluorescent signal upon titration with methimazole (Fig. 2f). This T-shaped Pi-stacking interaction in N61D mutant, is in line with its observed poor methimazole binding affinity (Table 2) and increased Pi-stacking distance (Fig. 2c).

In vitro experiments were carried out in the presence of indole to further characterize the observed differences in methimazole binding and the results are shown in Fig. 4a-c. As can be seen in Figure 4, the presence of indole suppresses methimazole S-oxidation. Especially for WT-hFMO3, 80% of the hFMO3 activity is inhibited in the presence of 4 mM indole (Figure 4a). This inhibition is also observed with N61Q and N61D mutants although N61D is again least affected i.e. only 20% inhibition by addition of 4 mM indole. In order to confirm that indole is acting as an inhibitor and that it cannot be metabolized by hFMO3 control experiments were carried out and the results are reported in Fig. S4a and b. These experiments consisted of NADPH consumption assay in presence of indole as well as HPLC analysis of the possible product of indole conversion by hFMO3. The results of both control experiments confirmed that indole is not a substrate of hFMO3.

To ascertain the type of inhibition of indole on hFMO3-mediated methimazole S-oxidation, inhibitory kinetics were studied using the double reciprocal Lineweaver-Burk plots and the data are shown in Fig. 4d. As can be seen from the plot, in the presence of increasing amounts of indole the K_m (slope of the straight lines) increases whereas the Vmax is unaffected (intercept of Y-axis), indicating that indole is a competitive

inhibitor of hFMO3 when methimazole is used as its substrate.

Taken together, *in silico* docking results are in line with the *in vitro* experimental data, showing that both indole and methimazole can competitively bind above the FAD isoalloxazine ring through Pi-stacking interaction, and that indole is a non-substrate competitive inhibitor of hFMO3.

3.3. Pre-steady-state and steady-state kinetic analysis of NADPH binding

As mentioned earlier, the hFMO3-mediated catalytic cycle contains both reductive and re-oxidative half reactions [29, 30]. As with any other enzyme, interfering with different steps of the catalytic cycle is consequential for the hFMO3 substrate oxygenation. For the reductive half-reaction, the pre-steady-state analysis using stopped-flow spectroscopy demonstrated that both N61Q and N61D mutations of hFMO3 decrease its NADPH binding affinity by 6- and 19-folds, respectively (Table 3). While for the catalytic constant (k_{red}) of flavin reduction, no significant changes were observed for these two mutants (Table 3).

Table 3 Michalis-Menten kinetic parameters determined for the reductive half-reaction of wild type and mutant hFMO3

	Reduction	
	K_d,NADPH *(μM)*	k_{red} (s^{-1})
Wild type [19]	0.30 ± 0.10	1.33 ± 0.03
N61D	5.89 ± 2.99	1.03 ± 0.11$^{\#}$
N61Q	1.85 ± 0.08	1.51 ± 0.40*

$^{\#}$P < 0.05, *P > 0.05 compared to WT hFMO3, one-way ANOVA followed by Student-Newman-Keuls test.

While for the steady-state kinetic experiments, Table 4 summarizes the K_m values for NADPH oxidase activities of the two mutants which show increases of 16- and 2.6-folds for N61D and N61Q, respectively. These higher K_m values are indicative of a decreased binding affinity for NADPH after mutation, which are in line with the higher K_d values reported in Table 3.

Table 4 Kinetic parameters of NADPH oxidation

hFMO3	K_m, NADPH *(μM)*	k_{cat}, NADPH *(μM/min/μM* enzyme)
WT [19]	14.96 ± 3.12	2.25 ± 0.20
N61D	239.17 ± 45.79**	15.18 ± 1.37***
N61Q	39.71 ± 12.77*	4.13 ± 0.66**

*P < 0.05, **P < 0.01, ***P < 0.001 compared to WT-hFMO3, one-way ANOVA followed by Student-Newman-Keuls test.

Pre-steady-state and steady-state kinetics show decreased NADPH affinity to the enzyme after mutation. In order to better understand the NADPH binding from a structural point of view, *in silico* docking experiments were carried out. Fig. 5 shows the binding modes of NADPH with WT-hMFO3 and its two mutants. The distances of residue 61 to flavin C4a and N5 monitored by DS Visualizer were used to measure the size of the oxygen reacting crevice. Fig. 5c shows that N61Q mutation results in an enlargement of the pocket whereas N61D mutation (Fig. 5b) has the opposite effect, although with a similar side-chain. The docking results display a disordered NADPH binding mode for N61D (Fig. 5b), similar to the one previously observed in N78D mutant of bFMO [31]. The crystal structures of bFMO [7] and yFMO [9] show that the $NADP^+$ amide group hydrogen bonds to flavin N5, and the nicotinamide sugar moiety is also within hydrogen-bond distance from the conserved Asn residue. If the latter conserved residue together with flavin N5 helps to guide and position NADPH binding, the disordered NADPH binding modes observed in the two mutants would rationalize the *in vitro* experimental data obtained i.e. decrease in NADPH binding affinity. Therefore, both *in silico* and *in vitro* data suggest that mutations of conserved amino acid 61 will result in poor NADPH binding affinity.

3.4. $NADP^+$ and Asn61 stabilize FAD intermediate

It is known that after flavin reduction by NADPH, the resulting $NADP^+$ stays bound

close to the FAD cofactor [6, 32]. The ITC data obtained for N61Q are shown in Fig. 6a with saturation at a molar ratio of around 10 resulting in a calculated K_d value of 56.3 μM. This value is an order of magnitude higher than the value previously reported for the WT hFMO3 (K_d of 3.7 μM) [19]. However, the data suggest that N61Q does still bind $NADP^+$.

On the other hand, experiments carried out with N61D mutant, demonstrate that titration with even higher concentrations of $NADP^+$, up to 20 mM, do not result in an observed binding curve (a higher concentration will result in a significant increase in heat of dilution), as shown in Fig. 6b. These data suggest that mutations of the Asn 61 cause changes in the binding affinity of $NADP^+$ and in the specific case of charge reversal, N61D, no binding is observed. The corresponding data of the wild-type hFMO3 has been recently reported by our group [19].

In general, as mentioned earlier, it is accepted that $NADP^+$ binds and remains in the active site of FMO stabilising the C4a-hydroperoxyflavin intermediate [6, 32]. Since the two mutants have poor $NADP^+$ binding affinity, the logical subsequent experiment was to investigate the stability of the FAD intermediates of N61D and N61Q. To this end, the formation and decay of C4a-hydroperoxyflavin intermediate of the two mutants was monitored by stopped-flow spectroscopy. Disproportionate increase in absorbance peaks at 381 nm and 450 nm (red spectra in Fig. 7a and b), are indicative of the intermediate formation and subsequent decay. As a consequence of the overlapping absorbance maxima around 381 nm of both FAD and C4a-hydroperoxyflavin intermediate (Fig. 7a), the intermediate was determined by the following equation (2) as previously reported [19].

$$A_{381(\text{Intermediate})} = (A_{381} - A_{650}) - (A_{450} - A_{650}) \times \frac{A_{381(\text{full reoxidation})} - A_{650(\text{full reoxidation})}}{A_{450(\text{full reoxidation})} - A_{650(\text{full reoxidation})}} \quad \text{(Eq. 2)}$$

No intermediate was observed for N61D mutant under the experimental conditions (Fig. 7b and d). In the case of N61Q mutant, compared to WT-hFMO3 [19], intermediate formation was not only slower but once formed, decayed faster indicative of the instability of this intermediate (Table 5).

Table 5 Kinetic parameters of C4a-hydroperoxyflavin intermediate stability in wild type and mutant hFMO3

hFMO3	Intermediate (381 nm)	
	$k_{formation}$ (s^{-1})	K_{decay} (s^{-1})
WT [19]	1.5801	0.0014
N61Q	0.8170	0.0038
N61D	Not detectable	

In the oxidative half-reaction, FMO requires the binding of $NADP^+$ to stabilize the C4a-(hydro)peroxyflavin before substrate access. Three features of the $NADP^+$ are well established: its nicotinamide moiety together with side chain of the conserved Asn residue and flavin C4a-N5 atoms define an O_2 reacting crevice [31]; proton transfer from the 2'-OH of the nicotinamide ribose to the C4a-peroxyflavin results in the formation of the C4a-hydroperoxyflavin; $NADP^+$ is stacked and hydrogen bonds with the isoalloxazine ring to protect the C4a-(hydro)peroxyflavin from decay [7, 31].

The docking results of $NADP^+$ shown in Fig. 8a illustrate that $NADP^+$, located above the isoalloxazine ring, together with Asn 61 shield flavin N5 and the C4a-hydroperoxide intermediate from solvent in the WT-hFMO3. While for the binding mode of N61D (Fig. 8b), the nicotinamide moiety is flipped out exposing the flavin N5 atom and its adjacent C4a-adduct intermediate to the solvent, which will lead to the destabilisation of the C4a-hydroperoxyflavin intermediate. In addition, the intermediate instability can be exacerbated by the repulsive interaction between the negatively charged side chain of N61D mutant and the C4a-hydroperoxide (Fig. 8b).

For N61Q mutant, the binding mode of $NADP^+$ is also altered although still on the side of flavin C4a-N5 with the bulkier glutamine side-chain stretching above the intermediate and shielding it in the same way as the WT (Fig. 8c).

These *in silico* data are in support of the experimental data where N61D mutation

converts the enzyme from a monooxygenase to an oxidase with undetectable C4a-hydroperoxyflavin intermediate (Fig. 7d), whilst the N61Q still has a detectable intermediate (Fig. 7c). Taken together, these data indicate $NADP^+$ together with the side-chain of Asn61 pose a protective barrier which is favourable for C4a-hydroperoxyflavin intermediate stability.

4. Discussion

In this work, the binding of substrate/inhibitor to hFMO3 was investigated both by means of *in vitro* as well as *in silico* experiments. Although the crystal structures of the yeast and bacterial FMOs were published more than a decade ago [7, 9], no structure is yet available for any of the human FMOs. In the absence of such structural information, site-directed mutagenesis (based on bacterial and yeast known structures) can confirm to some degree the correctness of available in silico 3D models, especially the catalytic pocket of the protein. Once the latter has been proven, as is the case in this work, docking experiments can be carried out to compare and contrast the binding of a substrate as opposed to an inhibitor and finally guide the development of hFMO3 inhibitors.

Literature data show that to date, only a very few true competitive inhibitors of FMO have been identified, and most of these compounds which lead to decrease FMO enzymatic activity are alternate substrate competitive inhibitors [33]. Cashman and his co-workers [33] reported indole-3-carbinol (I3C) and its acid-treated products, I33' and LT, as potent inhibitors of hFMO3. Methimazole is another known hFMO3 substrate and competitive inhibitor. To the best of our knowledge, the inhibitory mechanism of these compounds on hFMO3 have never been studied from a structural view point. The in vitro and in silico data presented in this work, demonstrates that the Pi-stacking interactions of these aromatic compounds to the isoalloxazine ring of the FAD cofactor is responsible for and contributes to the observed hFMO3 inhibition.

Future work will focus on the screening of aromatic chemicals in order to discover potential hFMO3 inhibitors with strong inhibitory effects, due to the striking association of hFMO3 inhibition with atherosclerosis treatment and prevention.

Conflict of interest

The authors declare no conflict of interest.

Acknowledgement

Chongliang Gao is the recipient of a three-year PhD scholarship from University of Torino for international students.

Author contributions

CG, GG and SJS designed the study. CG and GC carried out the experiments and collected the data. CG, GC and SJS analyzed and interpreted the data. CG, GG and SJS drafted and revised the manuscript. All authors have read and approved the final manuscript.

REFERENCES

[1] S.K. Krueger, D.E. Williams, Mammalian flavin-containing monooxygenases: structure/function, genetic polymorphisms and role in drug metabolism, Pharmacology & Therapeutics 106(3) (2005) 357-387.

[2] I.R. Phillips, E.A. Shephard, Drug metabolism by flavin-containing monooxygenases of human and mouse, Expert Opinion on Drug Metabolism & Toxicology 13(2) (2016) 167-181.

[3] G. Catucci, C. Gao, S.J. Sadeghi, G. Gilardi, Chemical applications of Class B flavoprotein monooxygenases, Rendiconti Lincei 28(S1) (2016) 195-206.

[4] S. Castrignanò, G. Gilardi, S.J. Sadeghi, Human Flavin-Containing Monooxygenase 3 on Graphene Oxide for Drug Metabolism Screening, Analytical Chemistry 87(5) (2015) 2974-2980.

[5] G. Catucci, I. Polignano, D. Cusumano, C. Medana, G. Gilardi, S.J. Sadeghi, Identification of human flavin-containing monooxygenase 3 substrates by a colorimetric screening assay, analytical biochemistry 522 (2017) 46-52.

[6] D.M. Ziegler, An overview of the mechanism, substrate specificities, and structure of FMOs, Drug Metabolism Reviews 34(3) (2002) 503-511.

[7] A. Alfieri, E. Malito, R. Orru, M.W. Fraaije, A. Mattevi, Revealing the moonlighting role of NADP in the structure of a flavin-containing monooxygenase, Proceedings of the National Academy of Sciences 105(18) (2008) 6572-6577.

[8] L.K. Siddens, S.K. Krueger, M.C. Henderson, D.E. Williams, Mammalian flavin-containing monooxygenase (FMO) as a source of hydrogen peroxide, Biochemical Pharmacology

89(1) (2014) 141-147.

[9] S. Eswaramoorthy, J.B. Bonanno, S.K. Burley, S. Swaminathan, Mechanism of action of a flavin-containing monooxygenase, Proceedings of the National Academy of Sciences 103(26) (2006) 9832-9837.

[10] S.K. Krueger, J.E. VanDyke, D.E. Williams, R.N. Hines, The Role of Flavin-Containing Monooxygenase (FMO) in the Metabolism of Tamoxifen and Other Tertiary Amines, Drug Metabolism Reviews 38(1-2) (2008) 139-147.

[11] Z. Wang, E. Klipfell, B.J. Bennett, R. Koeth, B.S. Levison, B. DuGar, A.E. Feldstein, E.B. Britt, X. Fu, Y.-M. Chung, Y. Wu, P. Schauer, J.D. Smith, H. Allayee, W.H.W. Tang, J.A. DiDonato, A.J. Lusis, S.L. Hazen, Gut flora metabolism of phosphatidylcholine promotes cardiovascular disease, Nature 472(7341) (2011) 57-63.

[12] M. Warrier, Diana M. Shih, Amy C. Burrows, D. Ferguson, Anthony D. Gromovsky, Amanda L. Brown, S. Marshall, A. McDaniel, Rebecca C. Schugar, Z. Wang, J. Sacks, X. Rong, Thomas de A. Vallim, J. Chou, Pavlina T. Ivanova, David S. Myers, H.A. Brown, Richard G. Lee, Rosanne M. Crooke, Mark J. Graham, X. Liu, P. Parini, P. Tontonoz, Aldon J. Lusis, Stanley L. Hazen, Ryan E. Temel, J.M. Brown, The TMAO-Generating Enzyme Flavin Monooxygenase 3 Is a Central Regulator of Cholesterol Balance, Cell Reports 10(3) (2015) 326-338.

[13] J.M. Brown, S.L. Hazen, The Gut Microbial Endocrine Organ: Bacterially Derived Signals Driving Cardiometabolic Diseases, Annual Review of Medicine 66(1) (2015) 343-359.

[14] J.A.P. Tomlinson, D.C. Wheeler, The role of trimethylamine N-oxide as a mediator of cardiovascular complications in chronic kidney disease, Kidney International 92(4)

(2017) 809-815.

[15] D.M. Shih, Z. Wang, R. Lee, Y. Meng, N. Che, S. Charugundla, H. Qi, J. Wu, C. Pan, J.M. Brown, T. Vallim, B.J. Bennett, M. Graham, S.L. Hazen, A.J. Lusis, Flavin containing monooxygenase 3 exerts broad effects on glucose and lipid metabolism and atherosclerosis, Journal of Lipid Research 56(1) (2015) 22-37.

[16] R.C. Schugar, J.M. Brown, Emerging roles of flavin monooxygenase 3 in cholesterol metabolism and atherosclerosis, Current Opinion in Lipidology 26(5) (2015) 426-431.

[17] G. Catucci, G. Gilardi, L. Jeuken, S.J. Sadeghi, In vitro drug metabolism by C-terminally truncated human flavin-containing monooxygenase 3, Biochemical Pharmacology 83(4) (2012) 551-558.

[18] S.J. Sadeghi, R. Meirinhos, G. Catucci, V.R. Dodhia, G. Di Nardo, G. Gilardi, Direct Electrochemistry of Drug Metabolizing Human Flavin-Containing Monooxygenase: Electrochemical Turnover of Benzydamine and Tamoxifen, Journal of the American Chemical Society 132(2) (2010) 458-459.

[19] C. Gao, G. Catucci, S. Castrignanò, G. Gilardi, S.J. Sadeghi, Inactivation mechanism of N61S mutant of human FMO3 towards trimethylamine, Scientific Reports 7(1) (2017).

[20] H.J. Cho, H.Y. Cho, K.J. Kim, M.H. Kim, S.W. Kim, B.S. Kang, Structural and functional analysis of bacterial flavin-containing monooxygenase reveals its ping-pong-type reaction mechanism, Journal of Structural Biology 175(1) (2011) 39-48.

[21] C. Gao, G. Catucci, G. Di Nardo, G. Gilardi, S.J. Sadeghi, Human flavin-containing monooxygenase 3: Structural mapping of gene polymorphisms and insights into molecular basis of drug binding, Gene 593(1) (2016) 91-99.

[22] E. Krieger, G. Vriend, Models@Home: distributed computing in bioinformatics using a screensaver based approach, Bioinformatics 18(2) (2002) 315 - 318.

[23] A. Gangjee, O.A. Namjoshi, S. Raghavan, S.F. Queener, R.L. Kisliuk, V. Cody, Design, Synthesis, and Molecular Modeling of Novel Pyrido[2,3-d]pyrimidine Analogues As Antifolates; Application of Buchwald–Hartwig Aminations of Heterocycles, Journal of Medicinal Chemistry 56(11) (2013) 4422-4441.

[24] G. Catucci, I. Zgrablic, F. Lanciani, F. Valetti, D. Minerdi, D.P. Ballou, G. Gilardi, S.J. Sadeghi, Characterization of a new Baeyer-Villiger monooxygenase and conversion to a solely N-or S-oxidizing enzyme by a single R292 mutation, Biochimica et Biophysica Acta (BBA) - Proteins and Proteomics 1864(9) (2016) 1177-1187.

[25] J.R. Lepock, K.P. Ritchie, M.C. Kolios, A.M. Rodahl, K.A. Heinz, J. Kruuv, Influence of transition rates and scan rate on kinetic simulations of differential scanning calorimetry profiles of reversible and irreversible protein denaturation, Biochemistry 31 (1992) 12706–12712.

[26] A.W.P. Vermeer & W. Norde, The thermal stability of immunoglobulin: Unfolding and aggregation of a multi-domain protein, Biophysical Journal 78, (2000) 394-404.

[27] C.T. Dolphin, A. Janmohamedb, R.L. Smithc, E.A. Shephard, I.R. Phillips, Compound heterozygosity for missense mutations in the flavin-containing monooxygenase 3 (FMO3) gene in patients with fish-odour syndrome, Pharmacogenetics 10(9) (2000) 799-807.

[28] D.H. Lang, C.K. Yeung, R.M. Peter, C. Ibarra, R. Gasser, K. Itagaki, R.M. Philpot, A.E. Rettie, Isoform specificity of trimethylamine N-oxygenation by human flavin-containing

monooxygenase (FMO) and P450 enzymes: Selective catalysis by fmo3, Biochemical Pharmacology 56(8) (1998) 1005-1012.

[29] B. Narlin B., D.P. Ballou, The reductive half-reaction of liver microsomal FAD- containing monooxygenases, Journal of Biological Chemistry 256 (1981) 4611-4618.

[30] B. Narlin B., D.P. Ballou, The oxidative half-reaction of liver microsomal FAD- containing monooxygenases, Journal of Biological Chemistry 256(9) (1981) 4619-4625.

[31] R. Orru, D.E.T. Pazmino, M.W. Fraaije, A. Mattevi, Joint Functions of Protein Residues and NADP(H) in Oxygen Activation by Flavin-containing Monooxygenase, Journal of Biological Chemistry 285(45) (2010) 35021-35028.

[32] J.A. Mayfield, R.E. Frederick, B.R. Streit, T.A. Wencewicz, D.P. Ballou, J.L. DuBois, Comprehensive Spectroscopic, Steady State, and Transient Kinetic Studies of a Representative Siderophore-associated Flavin Monooxygenase, Journal of Biological Chemistry 285(40) (2010) 30375-30388.

[33] J.R. Cashman, Y. Xiong, J. Lin, H. Verhagen, G.V. Poppel, P.J. Bladerent, S. Larsen-Su, D.E. Williams, In Vitro and In Vivo Inhibition of Human Flavin-Containing Monooxygenase Form 3 (FMO3) in the Presence of Dietary Indoles, Biochemical Pharmacology 58(6) (1999) 1047-1055.

Figure legends

Fig. 1 UV-Vis spectra (300-550 nm) of WT-hFMO3, N61Q and N61D. Protein spectra (3.5 μM) were recorded in 0.1 M phosphate buffer (pH 7.4), 20% glycerol, 1 mM EDTA.

Fig. 2 Docking results of hFMO3 with methimazole (MMI). (a) WT plus MMI; (b) N61Q plus MMI; (c) N61D plus MMI; Docking performed by YASARA structure package and results analyzed by DS Visualizer. The conventional hydrogen bond is in green, the Pi-Pi stacking interaction of MMI and isoalloxazine ring in magenta with the stacking distance indicated. FAD fluorescence changes upon MMI addition for (d) WT-hFMO3, (e) N61Q and (f) N61D.

Fig. 3 Co-crystal structures of (a) Indole-bFMO (PDB ID: 2XVJ) and (b) MMI-yFMO (PDB ID: 2GVC) show the substrate Pi-stacking with isoalloxazine ring of FAD and Pi-Pi interactions (T-shaped) with an aromatic residue nearby (cyan). Molecular docking experiment shows similar Pi-stacking binding mode in (c) MMI/hFMO3. Pi-Pi interactions are in black dotted lines, FAD in orange. The Pi-Pi interactions were monitored by DS Visualizer and figures were generated with PyMOL.

Fig. 4 Inhibition of the methimazole (MMI) S-oxygenation catalyzed by (a) WT-hFMO3, (b) N61Q and (c) N61D by indole and the type of enzyme inhibition determined by (d) Lineweaver-Burk plot (each data point is the mean from at least three experiments).

Fig. 5 Docking of NADPH to hFMO3 model (a) WT, (b) N61D and (c) N61Q. The distance from residue 61 side-chain to flavin C4a-N5 was measured by DS visualizer. NADPH is in yellow, FAD in magenta, residue 61 in green. Oxygen atoms are in red with nitrogen in blue. Docking performed by YASARA structure package.

Fig. 6 Isothermal titration calorimetry data for hFMO3 mutants (a) N61Q and (b) N61D binding with $NADP^+$. The experiments were performed by titration of $NADP^+$ (20 mM for N61D and 2 mM for N61Q) into the protein solution (20 μM).

Fig. 7 The re-oxidation spectra of reduced hFMO3 mutants: (a) N61Q and (b) N61D at three different time points. Kinetics of formation and decay of the C4a-hydroperoxyFAD intermediates followed at 381 nm: (c) N61Q and (d) N61D. The figure insets show the same absorbance for the first five seconds.

Fig. 8 Docking results of the C4a-hydroperoxyflavin intermediate with $NADP^+$ for hFMO3 (a) WT, (b) N61D and (c) N61Q. The –OOH group at flavin C4a position was modelled in the $NADP^+$-free protein followed by the docking with $NADP^+$. The best docking result with highest score was selected for analysis. FAD and amino acid 61 are displayed in dots showing the van der waals radii. $NADP^+$ is in yellow with FAD in cyan. Docking performed by YASARA structure package.

Supporting Information

Binding of methimazole and NADP(H) to human FMO3: in vitro and in silico studies

Chongliang Gao, Gianluca Catucci, Gianfranco Gilardi, Sheila J. Sadeghi *
Department of Life Sciences and Systems Biology, University of Torino, Italy

Table S1 DSC data for wild-type hFMO3 at different scan rates (heating rates) with the calculated Tm and ΔH values of the two observed peaks.

	Peak 1		Peak 2	
Heating rate	T_m (°C)	ΔH Kcal/mol	T_m (°C)	ΔH Kcal/mol
180 °C/h	50.53	59.9	55.96	25.8
90 °C/h	48.78	50.3	54.66	29.2
30 °C/h	45.09	11	49.02	38.4

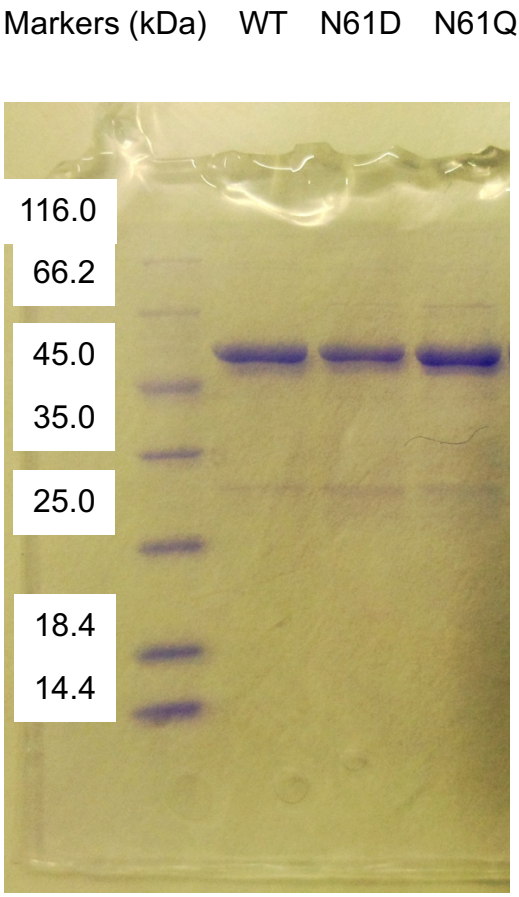

Figure S1 SDS-PAGE analysis of purified WT-hFMO3 and its two mutants N61D and N61Q. The protein band around 60 kDa is in good agreement with the theoretical molecular weight calculated from the amino acid sequence.

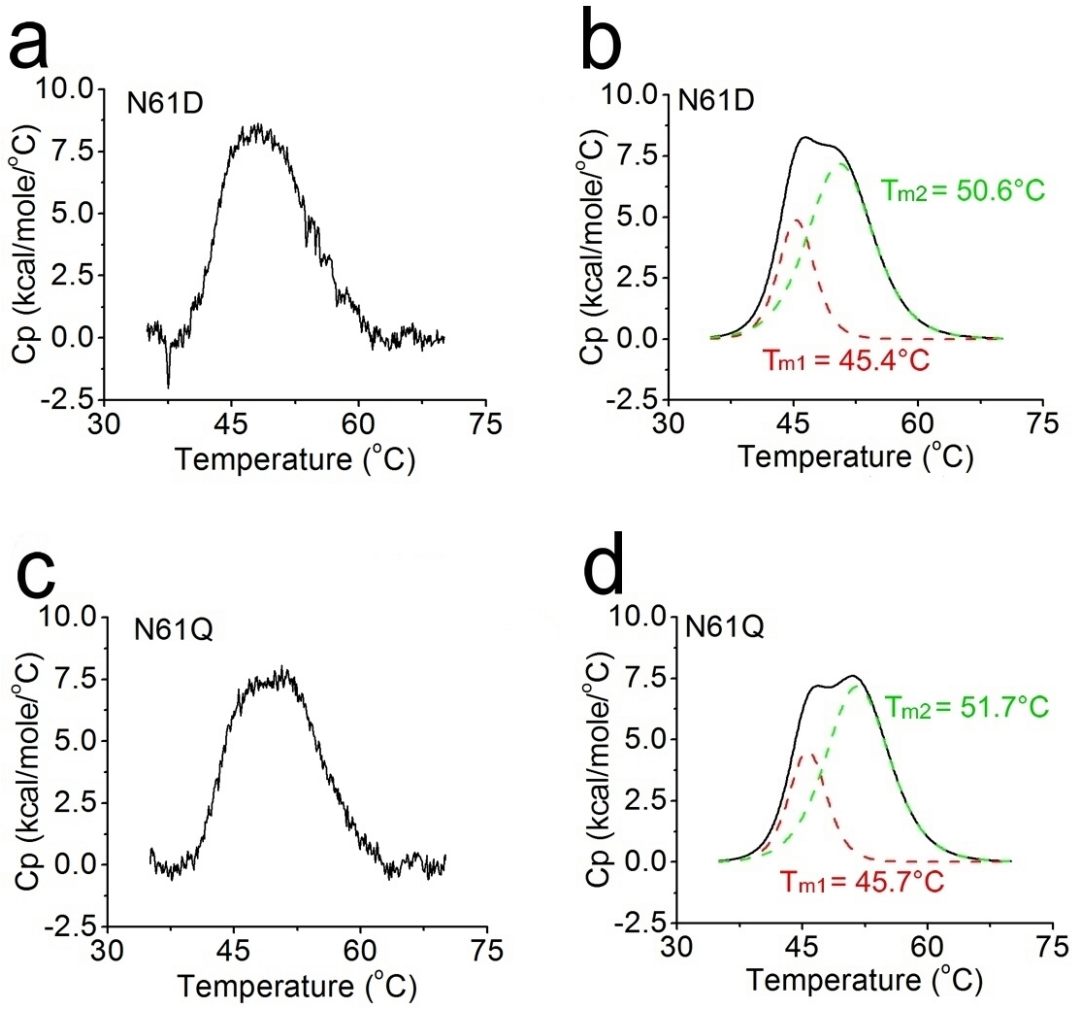

Figure S2 DSC data for (a) N61D and (c) N61Q mutants of hFMO3 together with the deconvoluted DSC profiles: (b) N61D; (d) N61Q. Protein concentration was 10 μM in 50 mM phosphate buffer, pH 7.4.

Figure S3 Michaelis-Menten curves of wild type and the two mutants of hFMO3.

Figure S4 (a)The superimposed HPLC chromatograms of the reaction of hFMO3 with indole after 30 minutes' incubation at 37 °C. (b) NADPH consumption assay by hFMO3 in the presence of different concentrations of indole.